ORIGINAL ARTICLE

Experimental study of the removal characteristics of C/SiC with different fiber structure arrangements for two-dimensional ultrasound-assisted grinding

Yashuai Wang[1] · Jiangtao Li[2]

Abstract

Ultrasound-assisted grinding is a new method for compound precision machining of C/SiC with excellent machining characteristics. The electroplated diamond grinding head performs a two-dimensional ultrasonic auxiliary plane grinding single-factor experiment for SiC, 2.5D-C/SiC, and chopped fiber-C/SiC. The influences of linear speed, feed speed, grinding depth, fiber orientation, and fiber structure on the grinding force and surface quality are analyzed in this study. The surface formation and removal mechanisms of C/SiC composites are discussed. The results show that within the parameters of this experiment, the grinding force and surface roughness decrease with the increase in linear speed and increase with the increase in feed speed and grinding depth. The grinding force and roughness can be significantly reduced by applying two-dimensional ultrasound. The maximum percentage reduction in normal and tangential grinding forces was 26.79% and 31.69% when grinding 2.5D-C/SiC along 90° fiber orientation. The maximum percentage of surface roughness reduction was 37.93% when 2.5D-C/SiC was ground along a 90° fiber orientation. The influence of fiber orientation on the two types of C/SiC grinding force is the same, and both are satisfied that the grinding force is highest in the 45° fiber orientation, second highest in the 90° fiber orientation, and lowest in the 0° fiber orientation. The effect of fiber orientation on the roughness of 2.5D-C/SiC is as follows: the surface roughness is highest at 45° fiber orientation, second highest at 90° fiber orientation, and lowest at 0° fiber orientation. The effect of fiber orientation on the roughness of short-cut fiber-C/SiC is as follows: the surface roughness is highest at 0° fiber orientation, second highest at 45° fiber orientation, and lowest at 90° fiber orientation. The effect of fiber structure on grinding force is as follows: Under the same machining conditions, the grinding forces are highest on SiC, second highest on short-cut fiber-C/SiC, and lowest on 2.5D-C/SiC. The effect of fiber structure on surface roughness is as follows: Under the same machining conditions, the surface roughness is highest on short-cut fiber-C/SiC, second highest on 2.5D-C/SiC, and lowest on SiC.

Keywords Ultrasound-assisted grinding · C/SiC composites · Fiber orientation · Grinding force · Surface quality

1 Introduction

With the rapid development of ultra-precision machining and intelligent manufacturing technology [1], some engineering ceramic parts have been widely used in automobiles, aircraft, spacecraft, and other fields [2–4]. Therefore, some

advanced processing methods and materials with excellent performance are born. Due to its excellent performance, silicon carbide has become the preferred choice for some special parts [5]. However, the high hardness and brittleness of SiC make secondary processing difficult [6, 7]. Carbon fiber-reinforced silicon carbide ceramic matrix composite (C/SiC) is a new material with high strength, high toughness, low density, high-temperature resistance, and wear resistance [8, 9], among which SiC is reinforced by carbon fiber to make up for the shortage of silicon carbide [10]. The two materials of 2.5D carbon fiber-toughened silicon carbide and chopped fiber toughened silicon carbide have high-cost performance. Although most of the C/SiC parts are directly produced using near-net forming technology [11].

✉ Yashuai Wang
1556543671@qq.com

1 School of Mechanical Engineering and Automation, Northeastern University, Shenyang, Liaoning 110819, China

2 Gongyi Fanrui Yihui Composite Material Co., Zhengzhou, Henan 451261, China

It is inevitable to improve the shape accuracy, dimensional accuracy, and surface accuracy of the parts through the grinding process [12]. The anisotropy and non-uniformity of C/SiC [13] will cause a large grinding force in conventional grinding (CG), resulting in poor surface quality and other problems [14]. Ultrasonic-assisted grinding has excellent grinding properties, such as small grinding force, good surface quality, less surface damage and defects, and high material removal rate [15–18].

In recent years, more and more scholars have researched the processing methods and material removal mechanism of C/SiC composites and have made some achievements. Zhang et al. [19] investigated the machining characteristics of C/SiC grinding assisted by one-dimensional axial ultrasonic applied to a tool. It was found that compared with conventional grinding, the normal force, tangential force, and surface roughness of ultrasonic-assisted grinding were reduced by about 20%, 18%, and 9%, respectively. However, the reduction percentage of grinding force and surface roughness in C/SiC grinding assisted by two-dimensional elliptical ultrasonic vibration has not been studied. Tian et al. [20–22] explored the grinding process from abrasive tools and developed a high-shear low-pressure composite materials dedicated abrasive system. On the inconel718 high-temperature alloy and nickel-based alloys, respectively, to do the grinding experimental research, the results show that the new abrasive tool has a high tangential force and low normal force of the grinding characteristics and significantly reduces the surface roughness to improve the surface quality. Liu et al. [23] investigated the influence of different fiber angles on the grinding of 2D-Cf/SiC and found that the fiber angle had a very important influence on the grinding force and surface quality of C/SiC and the fracture mode of the material. However, the effects of two-dimensional ultrasonic assisted grinding of 2.5D-C/SiC fiber angle on grinding force and surface roughness have not been studied. Xie et al. [24] investigated the influence of ultrasonic amplitude on the material removal mechanism during ultrasonic-assisted milling of 2.5D-C/SiC, and the results showed that ultrasonic-assisted machining could improve the surface quality and ultrasonic amplitude could improve the brittle fracture performance. Qu et al. [25, 26] explored the influence of grinding process parameters, fiber angle on grinding force, and surface roughness of grinding C/SiC. The fiber fracture mechanism was also analyzed to derive the material fracture mechanisms such as matrix cracking, fiber abrasion, interfacial debonding, fiber pull-out, and out-cropping. However, the lack of ultrasound-assisted grinding of C/SiC material removal mechanism was explored. Chen et al. [27] conducted experimental feasibility research and mechanism analysis on ultrasonic-assisted milling of 2D-Cf/SiC, and the results showed that machining parameters had a very important effect on cutting force and surface integrity,

and ultrasonic vibration could reduce milling temperature, reduced milling force, and improved surface quality. Luna et al. [28] investigated the influence of abrasive geometry and fiber orientation on the removal mechanism of SiC/SiC ceramic matrix composites, and the results showed that abrasive grain shape had a more important effect on the grinding force than fiber orientation in the removal process of brittle materials. A theoretical model for the variation of normal stress with contact length and during each cycle of ultrasonic vibration in UAT was derived by Jamshidi and Nategh [29]. It was found that all the forces in UAT vary with the time of cyclic separation and contact between the tool and the workpiece relative to the cutting speed. The reasons for the decrease in normal force and friction with increasing ultrasonic amplitude and frequency were also analyzed both theoretically and experimentally.

At present, most researchers mainly focus on the influence of fiber orientation on the surface quality or grinding force of a single type of C/SiC. Few have comprehensively compared the removal characteristics of 2.5D C/SiC, chopped fiber C/SiC, and SiC grinding. The machining method of applying two-dimensional ultrasonic assisted grinding (TDUAG) to the workpiece has a very significant advantage in the machining of C/SiC and SiC materials. The expansion of the processing method is of great significance in the application of C/SiC and SiC processing. Therefore, based on the method of applying two-dimensional ultrasonic vibration-assisted grinding to the workpiece. The experimental exploration of (TDUAG) and conventional grinding (CG) for these three materials was respectively carried out. The effects of linear speed, feed speed, grinding depth, fiber orientation, and toughening structure of carbon fiber on the grinding force, surface quality, and material removal mechanism are analyzed. This research is of great significance in expanding new methods for high efficiency, high precision machining of C/SiC and SiC.

2 Test conditions and theoretical analysis

2.1 Test conditions and workpiece materials

Grinding experiments are carried out on a type specification TCR 500 vertical machining center manufactured by Shenyang Machine Tool Factory. The experimental platform is shown in Fig. 1. The two-dimensional ultrasonic vibration platform is installed on the machine, and the clamping device is designed. The maximum speed of the TCR500 vertical machining center is 20000r/min, the machine table size is 650 mm × 400 mm, the positioning accuracy of the X-, Y-, and Z-axes is 0.01 mm, and the repeated positioning accuracy is 0.008mm. The grinding wheel adopts a 150-mesh, and a diameter of 25 mm electroplated diamond

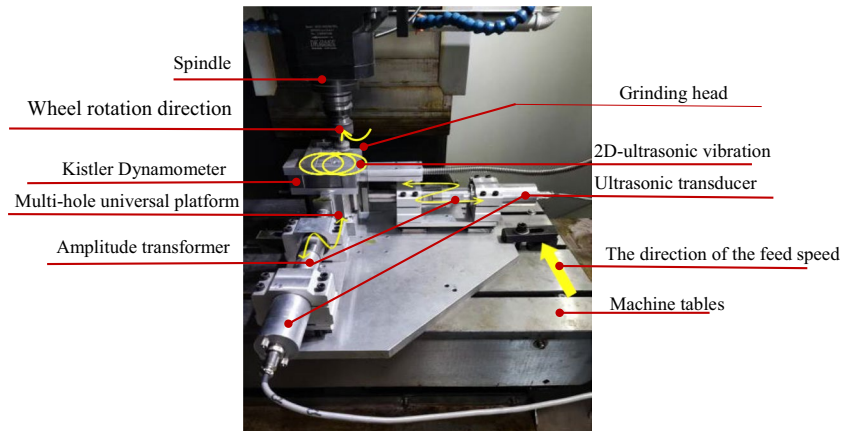**Fig. 1** Two-dimensional ultrasonic assisted grinding platform

Table 1 2.5D-C/SiC material parameter performance

Material parameters	Value
Tensile strength (MPa)	90–140
Curved strength (MPa)	160–240
Compress strength (MPa)	>220
Volume density (g/cm^3)	2.0

grinding head with a shank with a diameter is 10 mm. The two-dimensional ultrasonic vibration platform consists of an ultrasonic generator, two amplitudes, and transducers. The ultrasonic waves are generated from the two directions of X and Y, respectively, and then converge on the workpiece of the porous universal platform. The grinding forces during the experiment are recorded by the Six Degrees of Freedom Dynamometer Model 9119AA2 manufactured by Kistler of Switzerland. The dynamometer system consists of a piezoelectric crystal sensor, a 5080 charge amplifier, a 5697 data acquisition card, and a PC. The surface roughness Sa and the 3D profile of the grinding surface are measured using the NANOVEA ST400 3D non-contact surface topography measuring instrument manufactured by NANOVEA in the USA. The surface micrographs are taken with a 3D confocal laser microscope model OLS4100 manufactured by OLYMPUS. The surface microstructure is very important for the study of the grinding surface formation mechanism. The experimental materials are sintered silicon carbide ceramics, 2.5D-C/SiC, and chopped fiber-C/SiC composites. The workpiece size is $8 \times 8 \times 4$ mm. The parameter properties of the 2.5D C/SiC composites are given in Table 1. C/SiC composites for the fatal flaw that SiC are prone to brittle cracking, increasing its toughness and reducing the crack initiation and propagation rate during machining. 2.5D-C/SiC is based on the two-dimensional continuous fiber arrangement of X and Y; Z-direction needled fibers are added to connect each fiber layer. It has higher toughness than unidirectional continuous C/SiC and 2D-C/SiC, a more mature production process, and a lower production cost than 3D-C/SiC. The structure diagram of the 2.5D-C/SiC composite is shown in Fig. 2.

2.2 Experiment design and method

The previous investigation found that the main factors affecting the material removal were ultrasonic amplitude, linear speed, feed speed, grinding depth, and C/SiC fiber orientation. Therefore, a single-factor comparison experiment of SiC and C/SiC with (TDUAG) and (CG) is carried out using the electroplated diamond grinding heads dry-plane grinding method. The effects of process parameters, fiber orientation, and fiber structure on the grinding force and surface quality are investigated. The processing parameters are given in Table 2, and the grinding process diagram is shown in Fig. 3. Source selection of process parameters such as linear velocity, feed rate, and grinding depth. First, according to the previous exploration experiment, it was found that the interval between several levels of process parameters was relatively large. The experimental results will have a relatively obvious trend of change; if the interval is not large enough, accidental errors may be introduced to interfere with the experimental results; second, according to the performance parameters of the experimental platform machine tool itself. In Sect. 2.1 of the manuscript, the performance parameters of the machine tool TCR500 in this study are introduced in detail. Third, refer to the value of process parameters in relevant literature.

2.3 Mechanism analysis of ultrasonic-assisted grinding

In Fig. 4a, the grinding wheel performs a plane motion during grinding. The individual grit A on the grinding wheel is purely rolling with a curved trajectory. Its motion can be viewed as a combination of its rotation around point O and its movement along the Y-axis in parallel with point A. The

Fig. 2 Diagram of the 2.5D-C/ SiC three-dimensional structure
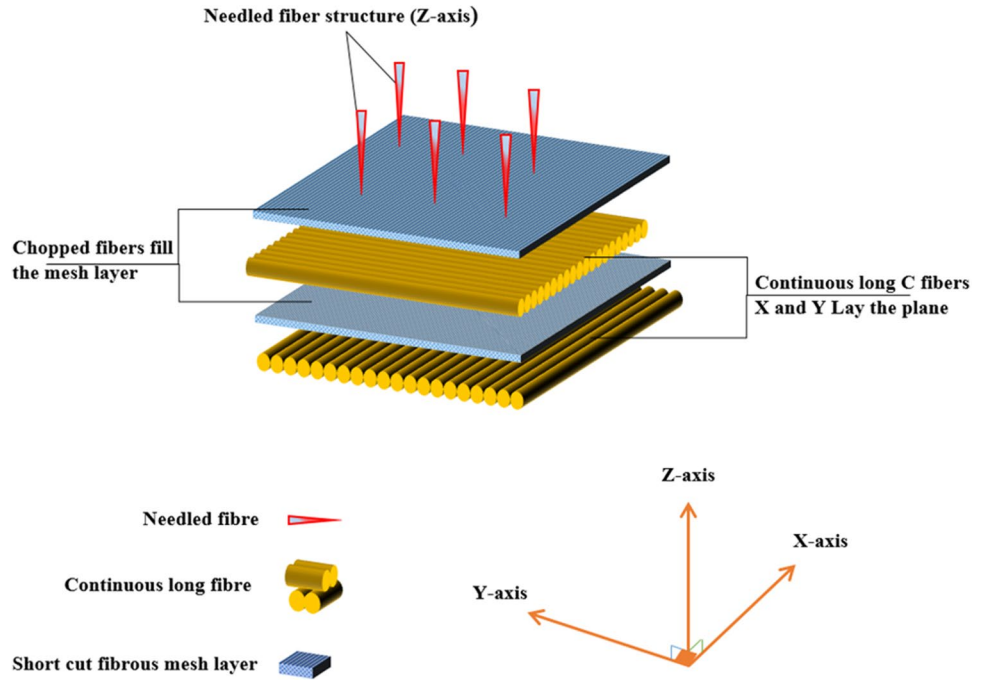
trajectory equation of the abrasive particle relative to the workpiece in the cutting process from point A to point B is as follows (1):

$$\begin{cases} X(t) = r - r \cdot \cos\phi = r \cdot (1 - \cos\omega t) \\ Y(t) = \delta s_w + r \cdot \sin\phi = v_w \cdot t + r \cdot \sin\omega t \end{cases} \quad (1)$$

By deriving the time t from Eq. (1) and Eq. (2), the velocity equations of a single grit without ultrasonic and ultrasonic-assisted grinding can be obtained as Eq. (3) and Eq. (4) respectively:

$$\begin{cases} v_x(t) = r \cdot \omega \cdot \sin\omega t \\ v_y(t) = v_w + r \cdot \omega \cdot \cos\omega t \end{cases} \quad (3)$$

where $X(t)$ and $Y(t)$ and v_x, v_y, v_z, and l_1, l_2 are the distance traveled from point A to point B, the velocity, and the arc length, respectively. r is the radius of the grinding wheel,

Figure 4b shows the trajectory diagram of a single diamond grit cut into the workpiece when 2D ultrasonic-assisted grinding is applied in the X and Y directions. The 2D ultrasonic trajectory is an ellipse when the phase angle is $\phi_1 = \phi_2 = 90°$. The equation of the motion trajectory after the ultrasonic application is shown in the following formula (2):

$$\begin{cases} X(t) = r \cdot (1 - \cos\phi) + A_1 \cdot \cos(\omega_1 t + \phi_1) = r - r \cdot \cos\phi + A_1 \cdot \sin\omega_1 t \\ Y(t) = v_w \cdot t + r \cdot \sin\phi + A_2 \cdot \cos(\omega_2 t + \phi_2) = v_w \cdot t + r \cdot \sin\phi + A_2 \cdot \sin\omega_2 t \end{cases} \quad (2)$$

$$\begin{cases} v_x(t) = r \cdot \omega \cdot \sin\omega t + A_1 \cdot \omega_1 \cdot \cos\omega_1 t \\ v_y(t) = v_w + r \cdot \omega \cdot \cos\omega t + A_2 \cdot \omega_2 \cdot \cos\omega_2 t \end{cases} \quad (4)$$

From this, it can be concluded that the contact arc length of a single grit in two-dimensional ultrasonic-assisted grinding with an applied phase angle of $\phi_1 = \phi_2 = 90°$ and without ultrasonic grinding is as follows (5):

$$\begin{cases} ls_1 = \int_0^t \sqrt{v_x^2 + v_y^2 + v_z^2} dt = \int_0^t \sqrt{(r \cdot \omega \cdot \sin\omega t)^2 + (v_w + r \cdot \omega \cdot \cos\omega t)^2} dt \\ ls_2 = \int_0^t \sqrt{v_x^2 + v_y^2 + v_z^2} dt = \int_0^t \sqrt{(r \cdot \omega \cdot \sin\omega t + A_1 \cdot \omega_1 \cos\omega_1 t)^2 + (v_w + r \cdot \omega \cdot \cos\omega t + A_2 \cdot \omega_2 \cdot \cos\omega_2 t)^2} dt \end{cases} \quad (5)$$

ϕ is the angle in radians at which the wheel turns from A to B, ω is the angular velocity of the wheel, and t is the time it takes for the wheel to turn from point A to point B.

Table 2 Processing test parameters

Process parameters	Value			
Linear speed v_s/(m/s)	0.66	2.36	10.48	23.56
Feed speed v_w/(mm/min)	5	20	50	100
Grinding depth a_p/(μm)	10	50	100	150

δs_w is the displacement of motion from O to O'. V_w is the feed speed. A_1, A_2 and ϕ_1, ϕ_2 and ω_1, ω_2 are the amplitude, phase angle, and angular frequency of vibration of the two-dimensional ultrasonic vibration platform in the X and Y directions, respectively.

According to the comparison of formula (5), the contact arc length of ultrasonic-assisted grinding is larger than that of non-ultrasonic grinding, thus reducing the grinding force. The specific quantitative analysis of l_{s1} and l_{s2} is as follows: Table 3 shows the specific values of processing parameters under the same conditions, where $\omega_1 = \omega_2 = 2\pi f_1 = 2\pi f_2, A_1 = A_2 = 10\mu m$.

The grinding time of a single grain is taken as $\pi/2$, π, $(3\pi)/2$, and 2π within 0–2π, respectively. Using the above formulae for the contact arc length of a single grain for conventional and 2D ultrasonically-assisted grinding and the values of the individual quantities, the values of l_1 and l_2 can be calculated as $l_1 = 4.91$, $l_2 = 5.16$, $l_1 = 9.82$, $l_2 = 10.32$, $l_1 = 14.73$, $l_2 = 15.48$, and $l_1 = 19.63$, and $l_2 = 20.64$. The 2D ultrasonic assisted grinding single particle contact arc length l_2 under the same conditions in each group is always larger than the conventional grinding single particle contact arc length l_1. This shows that 2D ultrasound-assisted grinding can increase the contact arc length of a single grain.

Each abrasive particle on the grinding wheel is regarded as a cutting edge, and the grinding surface is the result of the combined action of many continuous cutting edges. After two-dimensional ultrasound is applied, the trajectory of a single abrasive particle on the workpiece is changed by ultrasonic vibration in the X and Y directions, and the contact arc length between the abrasive particle and the workpiece

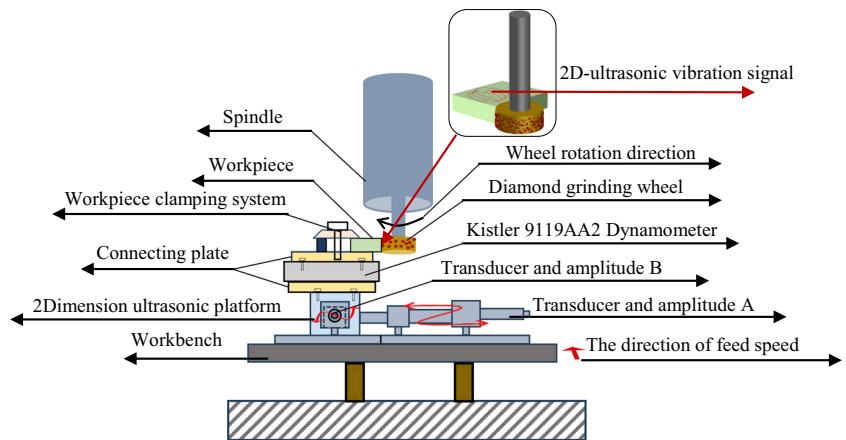**Fig. 3** Schematic diagram of ultrasonic assisted grinding device

Fig. 4 **a** Motion path diagram of a single grit in CG. **b** Motion path diagram of a single grit in TDUAG
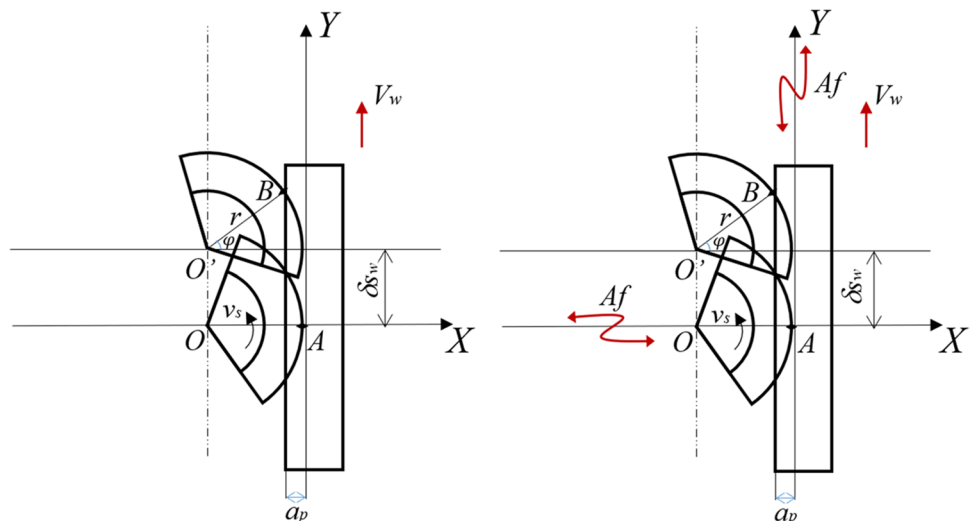
Table 3 Parameter values for calculating the contact arc length

Process parameters	(CG)	(TDUAG)
Angular speed of grinding wheel ω/(rad/s)	100	100
Radius of grinding wheel r/(mm)	25	25
Feed speed v_w/(mm/min)	100	100
Grinding time for a single grit t/(s)	$\pi/2, \pi, (3\pi)/2, 2\pi$	$\pi/2, \pi, (3\pi)/2, 2\pi$
Contact arc length of a single a single grit l/(mm)	4.91, 9.82,14.73, 19.63	5.16, 10.32, 15.48, 20.64
Ultrasound frequency f/(Hz)	20,000	20,000
Ultrasonic amplitude/(μm)	0	10

is increased. The volume of abrasive material removed per unit of time is fixed, and the average swarf area is inversely proportional to the contact arc length, so the average swarf area of a single abrasive particle is reduced after ultrasonic vibration is applied [30]. The grinding force of the abrasive particle is proportional to the sectional area of the chip, so the grinding force assisted by two-dimensional ultrasonic vibration is lower than that of ordinary grinding force [31]. At the same time, ultrasonic vibration also increases the number of cyclic contacts between the grain and the workpiece per unit of time.

The influence of the ultrasonic amplitude on the tangential grinding force and normal force in Fig. 5 shows that the grinding force is greatest without ultrasonic, and the grinding force decreases as the ultrasonic amplitude increases. When the ultrasonic amplitude is 10μm, the normal grinding force, and the tangential grinding force reach the minimum value, which is 5.9 N and 4.69 N, respectively. And the normal force is greater than the tangential force. This is because the grain have a large negative front angle, so increasing the ultrasonic amplitude can further increase the contact arc length of a single grain, and the average chip section area
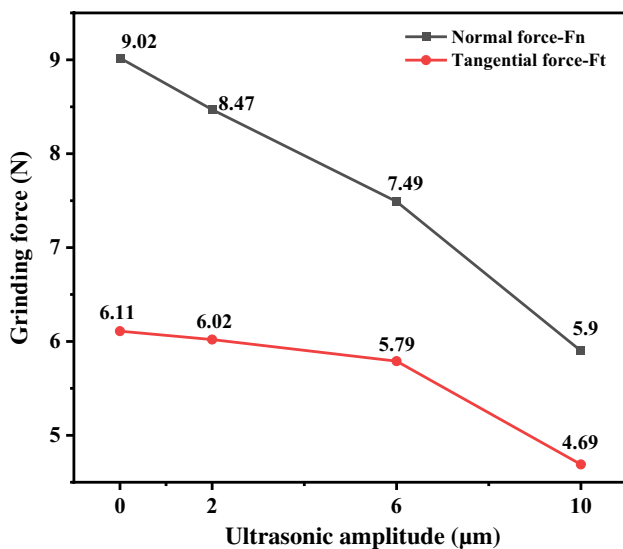
becomes smaller. Therefore, increasing the ultrasonic amplitude can reduce the grinding force.

Figure 6 shows a model diagram of a single abrasive particle being pressed into the ceramic. Figure 7 shows the schematic diagram of the surface cracking of engineering ceramics. According to indentation fracture mechanics, a central crack will appear on the surface when the load on the abrasive particles reaches a critical value [32]. When the abrasive particles are unloaded, the central crack closes but cannot be restored to its original state, and continuous
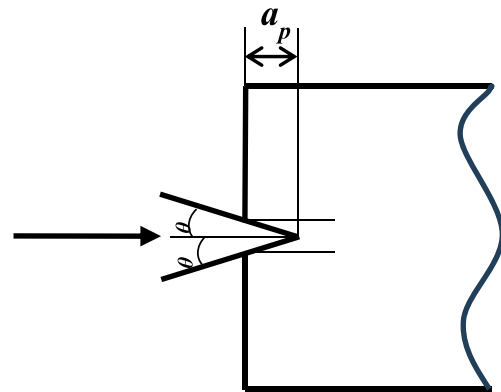

Fig. 6 Single grit is pressed into the workpiece model

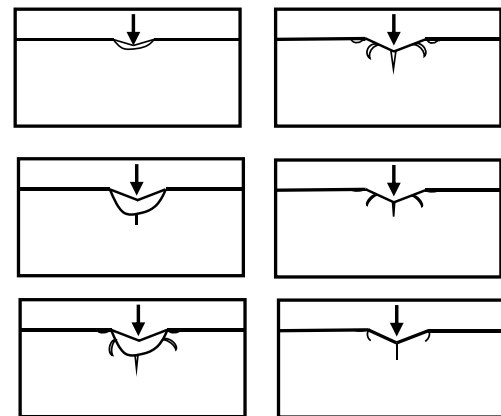**Fig. 5** Ultrasonic amplitude vs. grinding force

Fig. 7 Vickers indentation crack formation process [38]

unloading will produce transverse cracks under the action of tensile stress [33]. Two-dimensional ultrasound increases the frequency of the abrasive gratings per unit of time, resulting in periodic loading and unloading. Two-dimensional ultrasound increases the frequency of the abrasive cutters per unit of time, resulting in periodic loading and unloading [34]. In this process, the instantaneous cyclical force causes the material to undergo a small deformation, forming a plastic grinding zone that can produce a small transverse crack. These transverse cracks did not expand to form chips under the action of the high-frequency periodic grinding force and then formed a new grinding surface [35]. The high-frequency impact effect of the grinding area under high-frequency ultrasonic vibration is stronger, the micro-cracks are increased, the chip size is smaller, so the material is easier to remove, and the grinding force is reduced [36]. In addition, ultrasonic vibration shortens the time of abrasive action, and the delay in the outward expansion speed of the

loaded central crack is too late to expand so that the grinding surface can obtain a better surface quality [37]. Therefore, two-dimensional ultrasonic vibration-assisted grinding can improve surface quality.

3 Results and discussion

3.1 Grinding force

3.1.1 Linear speed

The feed speed is 50 mm/min, the grinding depth is 50 μm, and the linear speeds are 0.66m/s, 2.36m/s, 10.48m/s, and 23.6m/s respectively. Figure 8a–c, d–f, g shows the influence of linear speed on the grinding force at 0°, 90°, and 45° fiber orientation when ultrasonic-assisted and conventional grinding 2.5D-C/SiC, chopped fiber-C/SiC, and
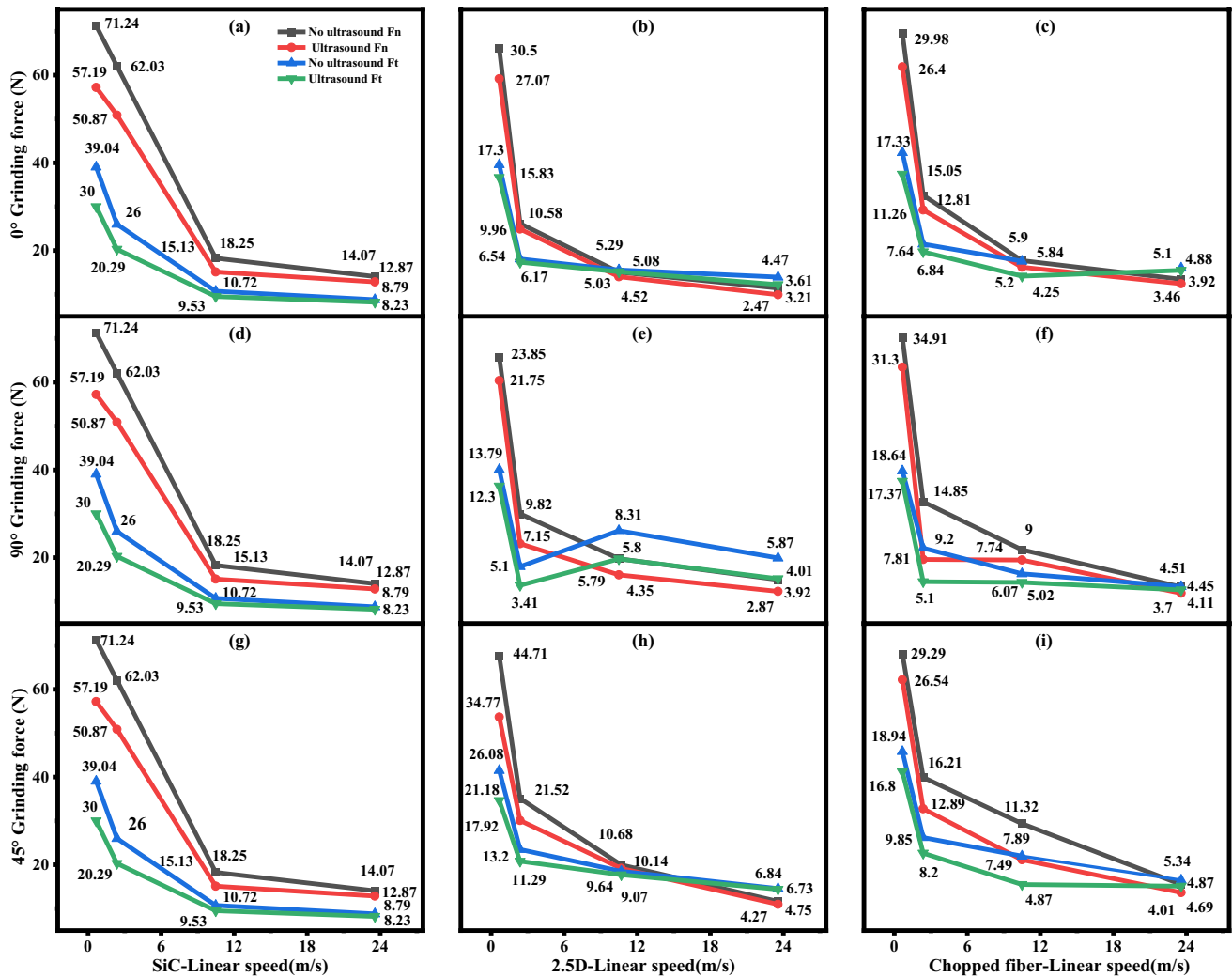

Fig. 8 Linear speed vs. grinding force

SiC respectively. When the linear speed increases from 0.66m/s to 23.6m/s, the normal and tangential grinding forces for grinding SiC decreased from 71.24 N and 39.04 N to 14.07 N and 8.79 N, respectively, while these after applying ultrasound decreased from 57.19 N and 30 N to 12.87 N and 8.23 N, respectively. The percentage reduction in normal and tangential grinding forces for applying ultrasound-assisted grinding of SiC compared to conventional grinding decreased from 19.72% and 23.15% to 8.23% and 6.37%, respectively. The normal and tangential forces in grinding 2.5D-C/SiC along the 0° fiber direction decreased from 30.5 N and 17.3 N to 3.21 N and 4.47 N, respectively, and after ultrasound is applied, these decreased from 27.07 N and 15.83 N to 2.47 N and 3.61 N, respectively. Compared with conventional grinding, the reduction of normal and tangential forces in the 0° fiber direction of 2.5D-C/SiC using ultrasonic-assisted grinding was 11.2%, 8.5%, 23.1%, and 19.24%, respectively. The normal and tangential forces in grinding 2.5D-C/SiC along the 90° fiber direction decreased from 23.85 N and 13.79 N to 3.92 N and 5.87 N, respectively, and after ultrasound was applied these decreased from 21.75 N and 12.3 N to 2.8 7N and 4.01 N, respectively. Compared with conventional grinding, the reduction of normal and tangential forces in the 90° fiber direction of 2.5D-C/SiC using ultrasonic-assisted grinding was 8.81%, 10.8%, 26.79%, and 31.69%, respectively. The normal and tangential forces in grinding 2.5D-C/SiC along the 45° fiber direction decreased from 44.71 N and 26.08 N to 4.75 N and 6.84 N, respectively, and after the ultrasound was applied, these decreased from 34.77 N and 21.18 N to 4.27 N and 6.73 N, respectively. Compared with conventional grinding, the reduction of normal and tangential forces in the 45° fiber direction of 2.5D-C/SiC using ultrasonic-assisted grinding is 22.23%, 18.79%, 10.11%, and 1.61%, respectively.

When the linear speed is increased from 0.66 m/s to 23.6 m/s for ultrasonic grinding of short-cut fiber-C/SiC along 0°, 90°, and 45° fiber orientations, the percentage reduction in normal and tangential forces, compared to conventional grinding are from 12.01% and 13.16% to 11.73% and 22%; from 10.34% and 6.81% to 17.96% and 7.64%; and from 9.39% and 11.30% to 17.66% and 12.17%.

The normal and tangential grinding forces on all surfaces decrease with increasing linear speed because of the increase in the number of diamond grits acting on the surface of the material when the linear speed increases. The feed speed of the grinding wheel per revolution is reduced, resulting in a reduction in the average thickness of the undeformed chips a_g of a single diamond abrasive particle, thus reducing the normal and tangential forces. The normal grinding force is greater than the tangential grinding force for all three materials in both ultrasonic and conventional grinding because

the diamond grits have a larger negative rake angle and flute radius. Applying 2D ultrasound reduces the grinding forces. The maximum percentage reduction in normal and tangential grinding forces is 26.79% and 31.69%, respectively, when grinding 2.5D-C/SiC along 90° fiber orientation.

3.1.2 Feed speed

The linear speed is 10.48 m/s, the grinding depth is 50 μm, and the feed speed is 5 mm/min, 20 mm/min, 50 mm/min, and 100 mm/min. Figure 9a–c, d–f, g shows the influence of feed speed on the grinding force at 0°, 90°, and 45° fiber orientation when grinding 2.5D-C/SiC, chopped fiber-C/SiC, and SiC, respectively.

When the feed speed is increased from 5 mm/min to 100 mm/min, the normal and tangential grinding forces of conventional and 2D ultrasound-assisted grinding of SiC increased from 8.87 N, 6.15 N and 6.35 N, 5.02 N to 30.66 N, 15.01 N and 21.9 N, 11.49 N, respectively. The application of 2D ultrasound resulted in a percentage reduction in normal and tangential grinding forces from 28.41% and 18.37% to 28.57% and 23.45% respectively. The normal and tangential forces increased from 3.49 N, 2 N and 2.64 N, 1.81 N to 8.81 N, 4.76 N and 6.5 N, 4.23 N, respectively, when conventional and 2D ultrasound-assisted grinding of 2.5D-C/SiC along 0° fiber orientation. Two-dimensional ultrasound resulted in a percentage reduction in normal and tangential grinding forces from 24.36% and 9.5% to 26.22% and 11.13%, respectively. The normal and tangential forces increased from 3.78 N, 3.49 N and 2.84 N, 2.7 N to 8.14 N, 10.61 N and 6.18 N, 7.6 N, respectively, when conventional and 2D ultrasound-assisted grinding of 2.5D-C/SiC along 90° fiber orientation. Two-dimensional ultrasound resulted in a percentage reduction in normal and tangential grinding forces from 24.87% and 22.64% to 24.08% and 28.37%, respectively. The normal and tangential forces increased from 5.51N, 5.1N and 3.86N, 3.57N to 15.47N, 12.2N and 11.85N, 10.85N, respectively, when conventional and 2D ultrasound-assisted grinding of 2.5D-C/SiC along 45° fiber orientation. Two-dimensional ultrasound resulted in a percentage reduction in normal and tangential grinding forces from 29.95% and 30% to 23.40% and 11.07%, respectively.

Figure 9 shows that both normal and tangential grinding forces increase with increasing feed speed. As the feed speed v_w increases, the relative contact area between the grit and the workpiece increases. Therefore, the maximum thickness of undeformed chips increases, and the total amount of material removed increases at the same time, increasing the grinding force. The normal and tangential forces after ultrasonic-assisted grinding are lower than those without ultrasonic. When the feed speed is taken as 5 mm/min for grinding 2.5D-C/SiC along 45° fiber orientation, the maximum percentage reduction in normal and tangential grinding
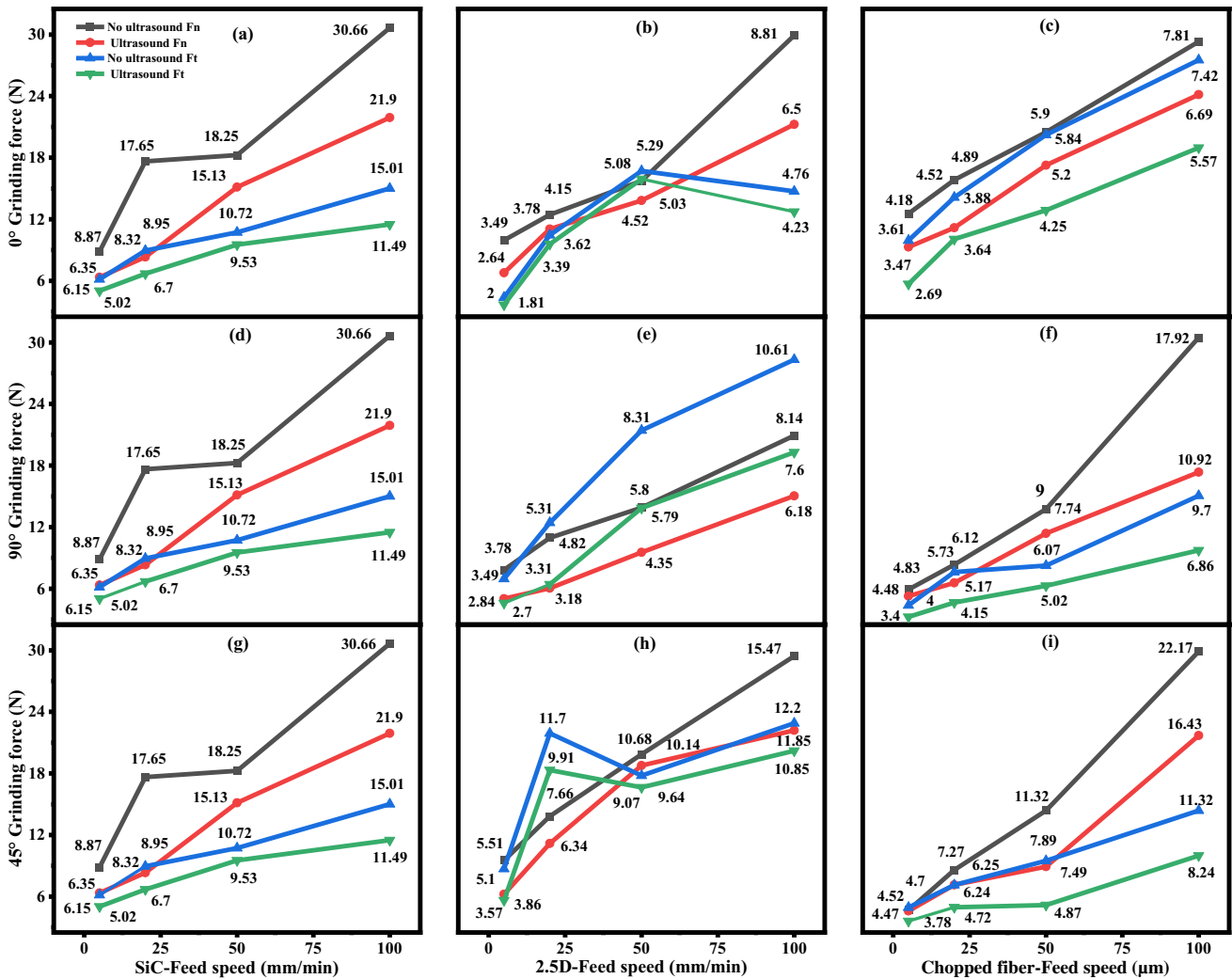
Fig. 9 Feed speed vs. grinding force

forces are 29.95% and 30%, respectively, and the reason for this phenomenon is discussed in the previous section. Due to the anisotropy and inhomogeneity of C/SiC materials, the mechanical properties of the materials are not the same in all directions of the fibers, so the trend of the grinding force increasing with the feed speed is not linear.

3.1.3 Grinding depth

When the linear speed is 10.48m/s and the feed speed is 50mm/min, the grinding depth values are 10 μm, 50 μm, 100 μm, and 150 μm. Figure 10a–c, d–f, and g shows the influence of grinding depth on the grinding force at 0°, 90°, and 45° fiber orientation when grinding 2.5D-C/SiC, chopped fiber-C/SiC, and SiC.

As the grinding depth increases from 10 μm to 150 μm, the normal and tangential grinding forces of conventional and 2D ultrasound-assisted grinding of SiC increased from

7.3 N, 4.51 N and 6.33 N, 4.05 N to 32.93 N, 17.55 N and 21.39 N, 12.3 N, respectively. The application of 2D ultrasound resulted in a percentage reduction in normal and tangential grinding forces from 13.29% and 10.20% to 35.04% and 29.91% respectively. The normal and tangential forces increased from 3.36N, 2.86N and 2.85N, 2.68N to 14.04N, 8.28N and 10.04N, 6.29N, respectively, when conventional and 2D ultrasound-assisted grinding of 2.5D-C/SiC along 0° fiber orientation. Two-dimensional ultrasound resulted in a percentage reduction in normal and tangential grinding forces from 15.18% and 6.29% to 28.49% and 24.03%, respectively. These forces increased from 3.84 N, 3.28 N and 3.12 N, 2.91 N to 9.93 N, 11.09 N and 7.84 N, 7.81 N, respectively, when grinding 2.5D-C/SiC along a 90° fiber orientation. The ultrasonic reduction percentages are 18.75% and 11.28% to 21.05% and 29.58%, respectively. These forces increased from 5.61 N, 5.16 N and 4.44 N, 4.03 N to 20.34 N, 14.35 N and 11.85 N, 10.9 N, respectively,
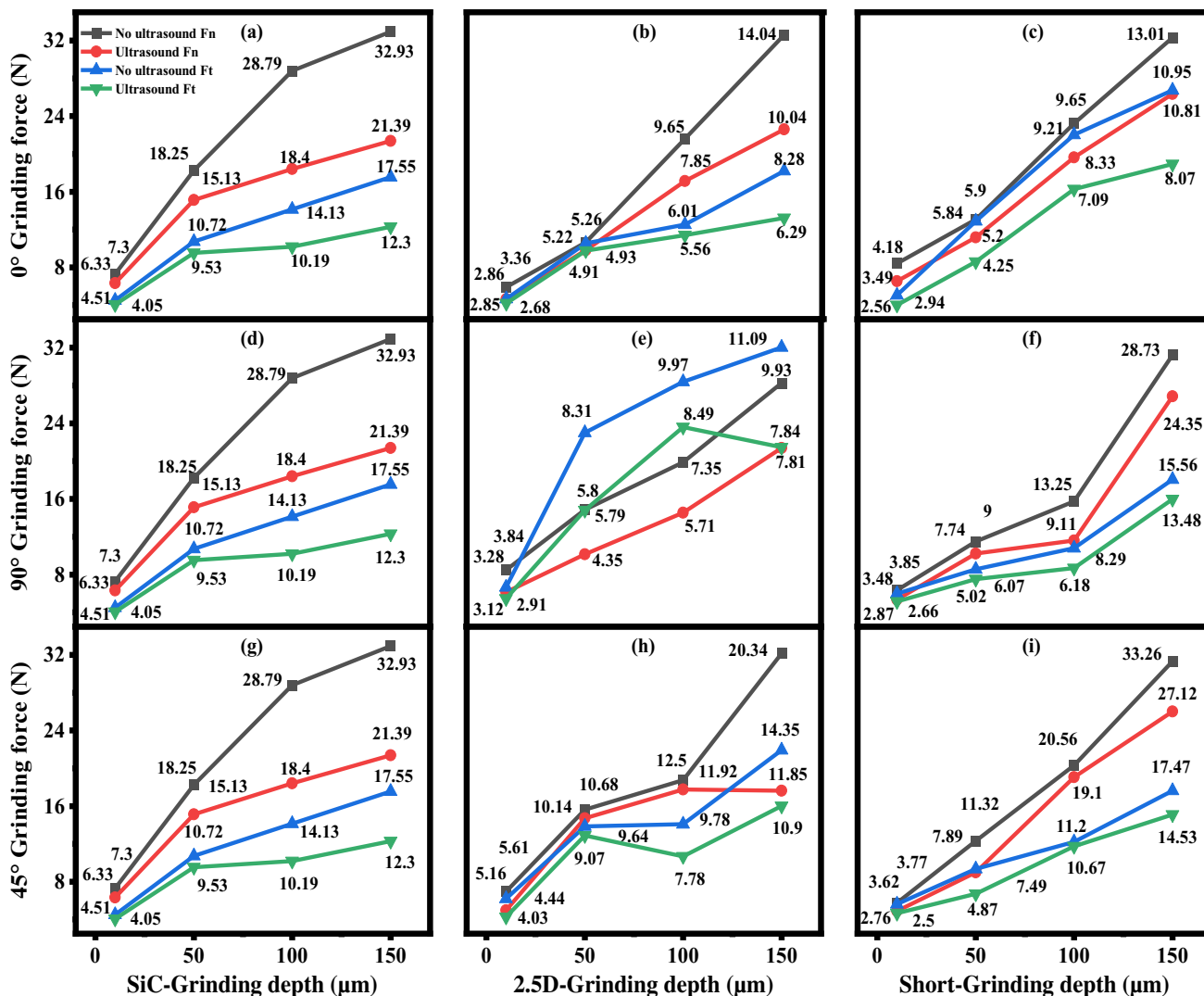
Fig. 10 Grinding depth vs. grinding force

when grinding 2.5D-C/SiC along a 45° fiber orientation. The ultrasonic reduction percentages are 20.86% and 21.90% to 41.74% and 24.04%, respectively.

Figure 10 shows that both normal and tangential grinding forces increase as the grinding depth increases. Because the maximum undeformed chip thickness of a single grit increases as the grinding depth increases during grinding. At the same time, the number of effective grits involved in grinding increases, increasing the grinding force.

3.2 Surface quality

3.2.1 Linear speed

Under the conditions shown in Table 2, the feed speed and the grinding depth remain unchanged at 50 mm/min and 50μm. The linear speed is varied. The effect of linear speed

on surface roughness during ultrasonic-assisted grinding and conventional grinding of 2.5D-C/SiC chopped fiber-C/SiC and SiC is investigated. The surface roughness S_a measured by NANOVEA ST 400 3D non-contact surface morphometry is shown in Fig. 11. Figure 11 shows the effect of linear speed on surface roughness when 2.5D-C/SiC, chopped fiber-C/SiC, and SiC are ground at 0°, 90°, and 45° angles between fiber and grinding directions respectively. As the linear speed increases, the surface roughness S_a decreases. The average thickness of undeformed chips a_g of a single grit decreases as the linear speed *vs.* in the grinding process increases, thus reducing the surface roughness.

To further demonstrate the influence of linear speed on C/SiC surface quality, the 3D profile of the grinding surface is recorded using NONAVEA topography. Figure 12 shows the law of the influence of linear speed on the 3D profile when grinding a 2.5D C/SiC transverse surface. The feed

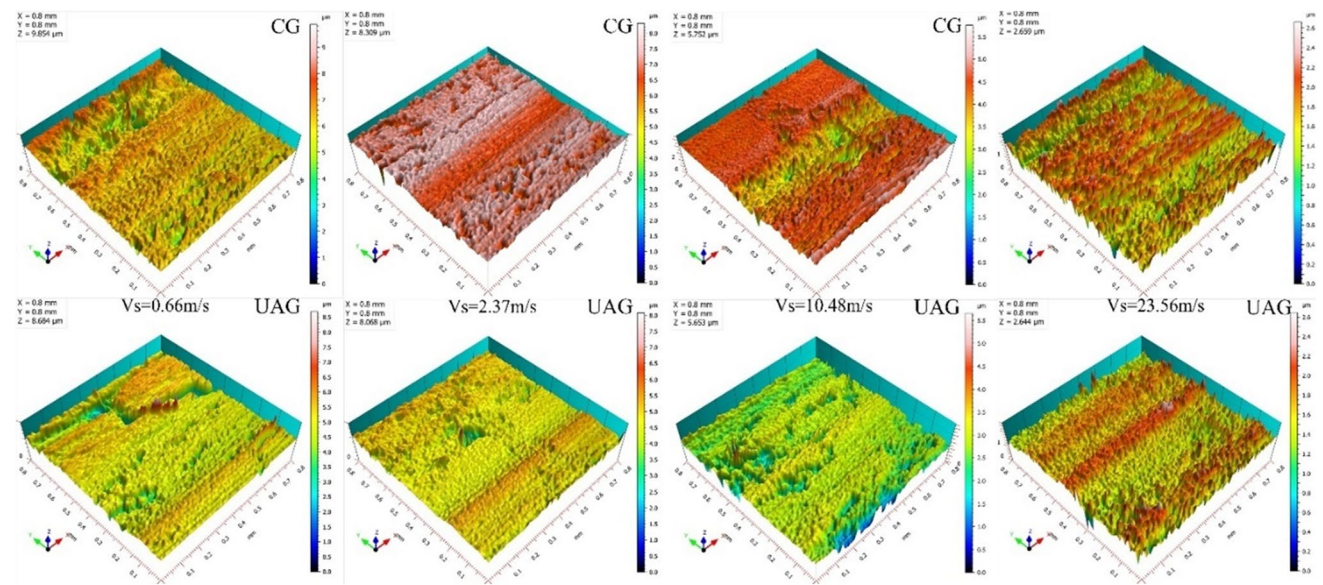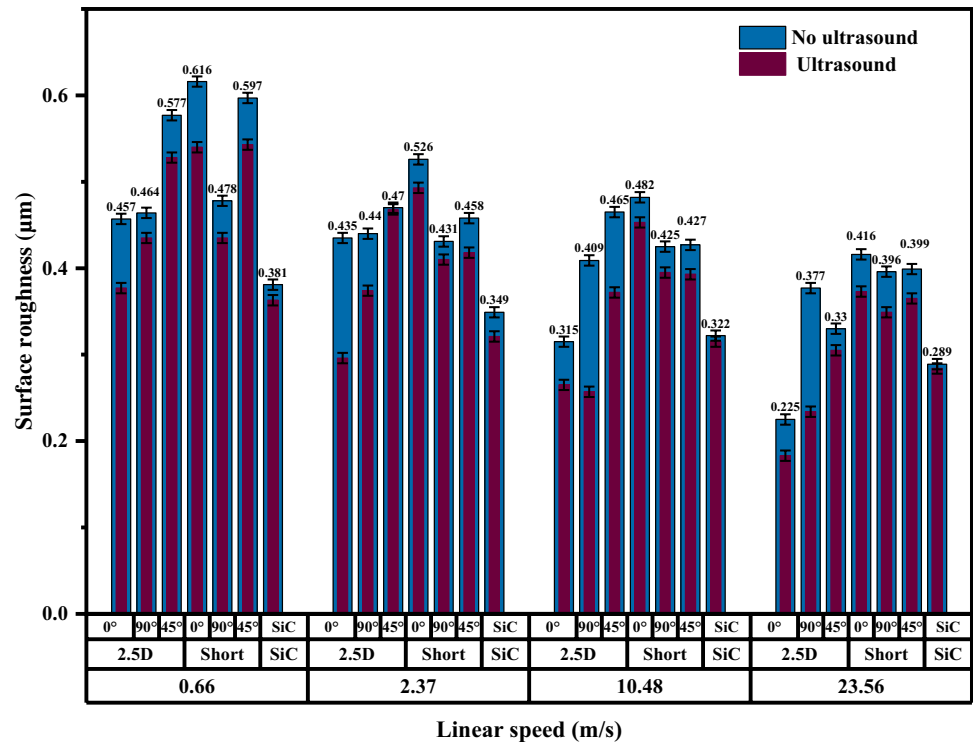**Fig. 11** Linear speed vs. surface roughness

Fig. 12 Linear speed vs. surface morphology

speed is 50 mm/min and the grinding depth is 50 μm. The linear speed is 0.66 m/s, 2.37 m/s, 10.48 m/s, and 23.56 m/s. Figure 12 clearly shows that the three-dimensional contour topography with a linear speed of 0.66m/s has the highest degree of concavity and the worst surface quality. As the linear speed increases, the surface roughness gradually improves and the height of the maximum convex surface and the depth of the minimum concave surface both show

a decreasing trend. The surface quality of the 3D profile is the best when the linear speed is 23.56m/s. Under the same machining parameters, the above figure is (CG) and the following figure is (TDUAG) profile. The degree of surface waviness after ultrasonic is smaller than that without ultrasonic. This result is fully consistent with the previous analysis of the influence of ultrasonic and linear speed on surface roughness and further confirms the view that increasing

linear speed reduces surface roughness, and ultrasonic can reduce surface roughness and improve surface quality. In the process of investigating the effect of line speed on surface roughness, the maximum percentage of ultrasound-assisted machining to reduce surface roughness is 37.93%, at which time the line speed for grinding 2.5D-C/SiC along 90° fiber orientation is taken as 10.48 m/s. The minimum percentage

of reduction in surface roughness is 1.7%, at which time the line speed is taken as 23.56 m/s for grinding SiC.

3.2.2 Feed speed

The linear speed is 10.48 m/s, the grinding depth is 50 μm and the feed speed is varied to investigate the effect of feed

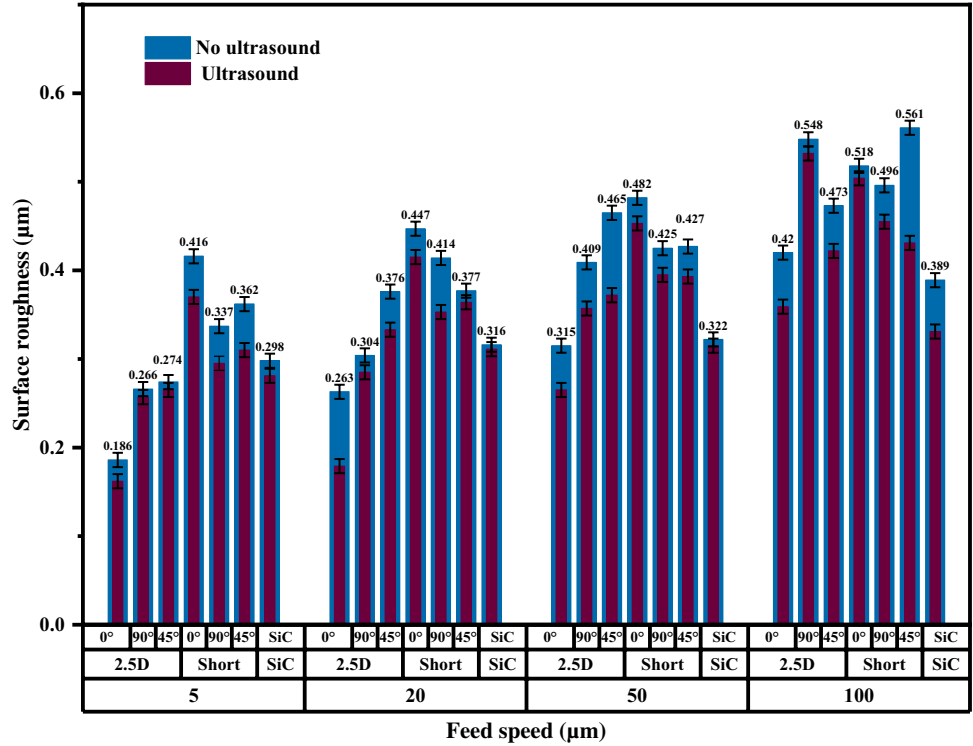**Fig. 13** Feed speed vs. surface roughness
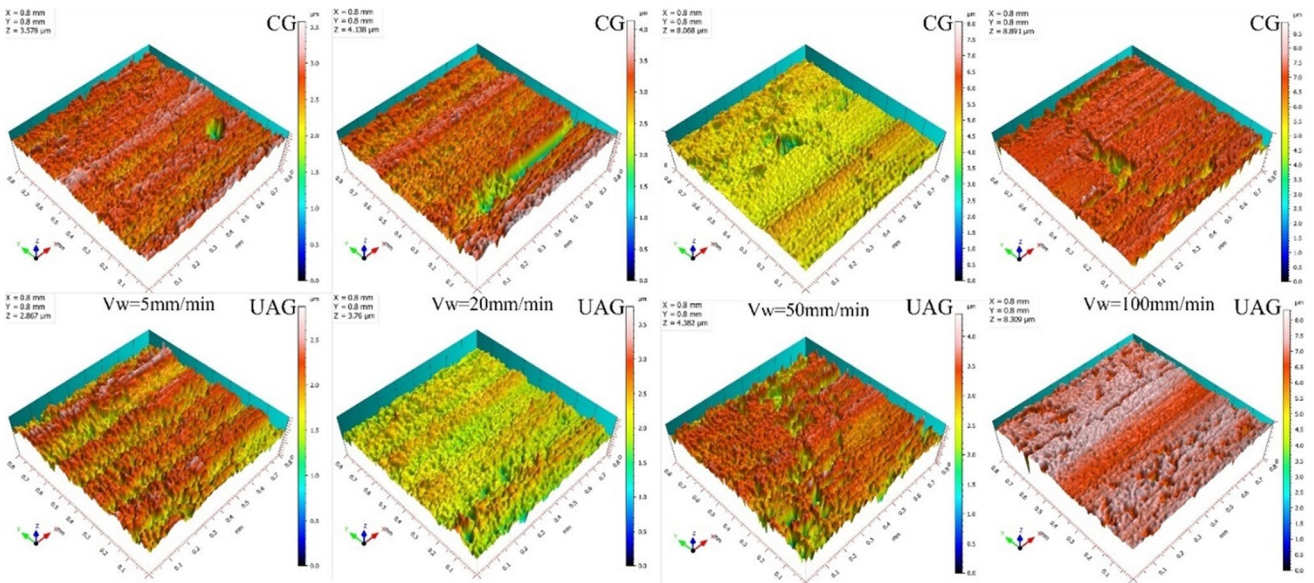
Fig. 14 Feed speed vs. surface morphology

speed on surface roughness. Figure 13 shows the effect of feed speed on roughness at 0°, 90°, and 45° fiber orientation when grinding 2.5D-C/SiC, chopped fiber-C/SiC, and SiC. The surface roughness S_a increases as the feed speed increases. As the feed speed v_w increases, the number of grits on the ground surface per unit of time decreases, and the surface roughness value S_a increases.

Figure 14 shows the effect of feed speed on the 3D profile of the surface when grinding 2.5D-C/SiC. The linear speed is 10.48 m/s, and the grinding depth is 50 μm. The feed speed is 5 mm/min, 20 mm/min, 50 mm/min, and 100 mm/min. At a feed speed of 5 mm/min, the degree of roughness of the contour map changes little, the pits are fewer and shallower, and the surface quality is better. As the feed speed increases, the surface roughness becomes worse, the height of the maximum bulge and the depth of the minimum pit both tend to increase, and more pits appear. The surface quality of a 3D profile with a feed speed of 100 mm/min is the worst.

In the process of investigating the influence of feed speed on surface roughness, the maximum percentage of ultrasound-assisted machining to reduce surface roughness is 23.17%, at this time along the 45° fiber orientation grinding chopped fiber-C/SiC feed speed of 100mm/min. The minimum percentage of reduction in surface roughness is 1.6% at this time for the grinding of SiC feed speed of 10mm/min.

3.2.3 Grinding depth

The linear speed is 10.48 m/s, the feed speed is 50 mm/min, and the grinding depth is varied to investigate the effect of grinding depth on surface roughness. Figure 15 shows the effect of grinding depth on roughness at 0°, 90°, and 45° fiber orientation when grinding 2.5D-C/SiC, chopped fiber-C/SiC, and SiC. Figure 15 shows that the surface roughness S_a increases as the grinding depth increases. As the grinding depth a_p increases, the thickness of the undeformed chips of a single abrasive particle increases, and the roughness value S_a increases. In the process of investigating the effect of grinding depth on surface roughness, the maximum percentage of ultrasonic-assisted machining to reduce surface roughness is 28.31%, at this time along the 0° fiber orientation grinding 2.5D-C/SiC grinding depth of 150mm/min. The minimum percentage of reduction in surface roughness is 2.17% at this time for grinding SiC grinding depth of 50μm.

Figure 16 shows the effect of the grinding depth on the 3D profile of the surface when grinding 2.5D-C/SiC. The linear speed is 10.48 m/s, and the feed speed is 50mm/min. The grinding depth is 10 μm, 50 μm, 100 μm, and 150 μm. The surface of the profile with the minimum grinding depth of 10μm has less concave and convex degrees, fewer shallow pits, and better surface quality. As the grinding depth increases, the surface roughness gradually worsens, the

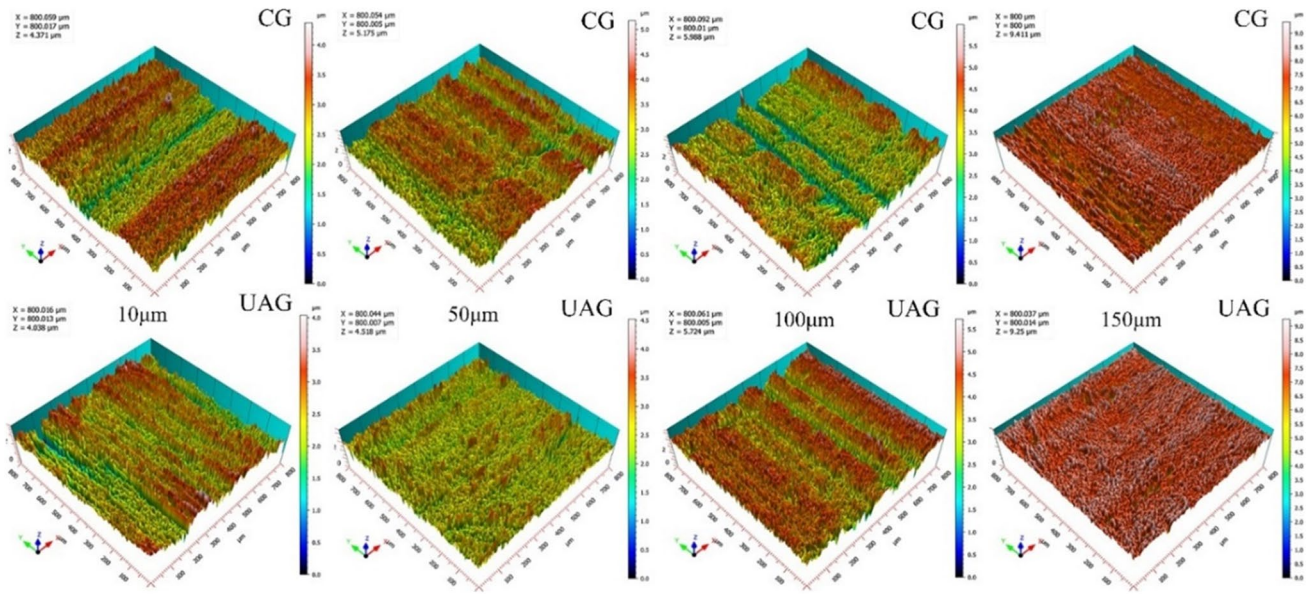**Fig. 15** Grinding depth vs. surface roughness
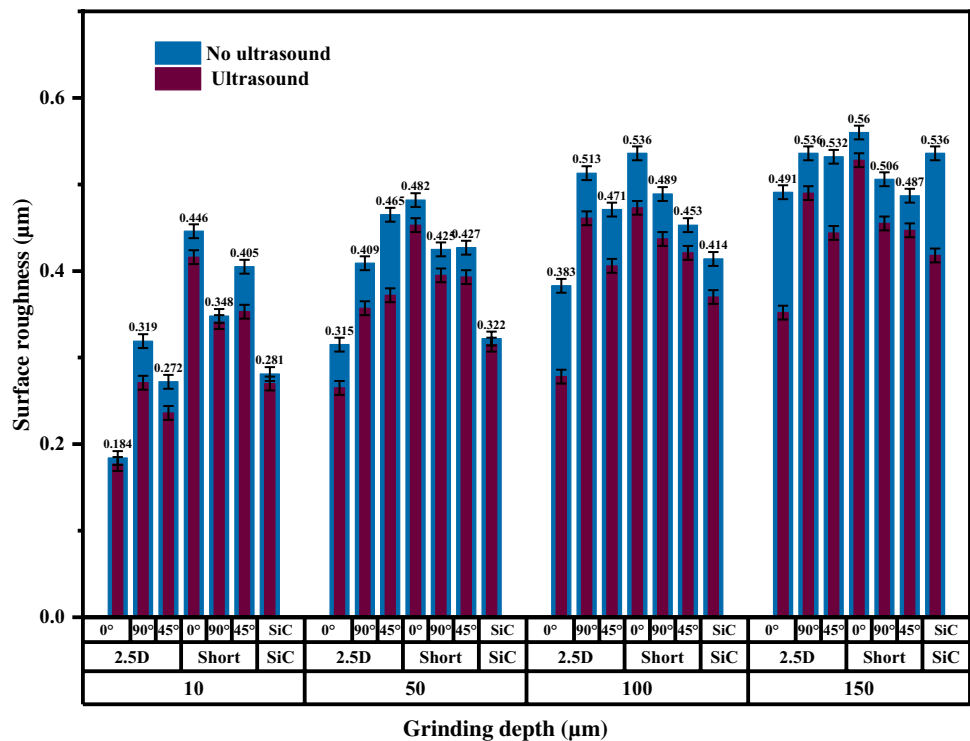
Fig. 16 Grinding depth vs. surface morphology

height of the maximum dent and the depth of the minimum pit both tend to increase, and more pits appear. The 3D profile with a maximum grinding depth of 150μm has the worst surface quality. Under the same machining parameters, the above figure is (CG), and the following figure is (TDUAG) contour. The fluctuation degree of the ultrasonic surface is smaller than that without ultrasonic, which further confirms the view that increasing the grinding depth can increase the surface roughness, and ultrasonic can reduce the surface roughness.

3.3 Effect of fiber orientation on force and surface

3.3.1 Effect of fiber orientation on force

For the same processing parameters, they are changing the orientation of the fibers. Figure 17a, b shows the influence of fiber orientation on the grinding force of 2.5D C/SiC and chopped fiber C/SiC composites respectively. Figure 17 shows that the grinding force of 45° fiber orientation is greater than that of 90° fiber orientation, and the grinding

Fig. 17 C/SiC fiber orientation vs. grinding force
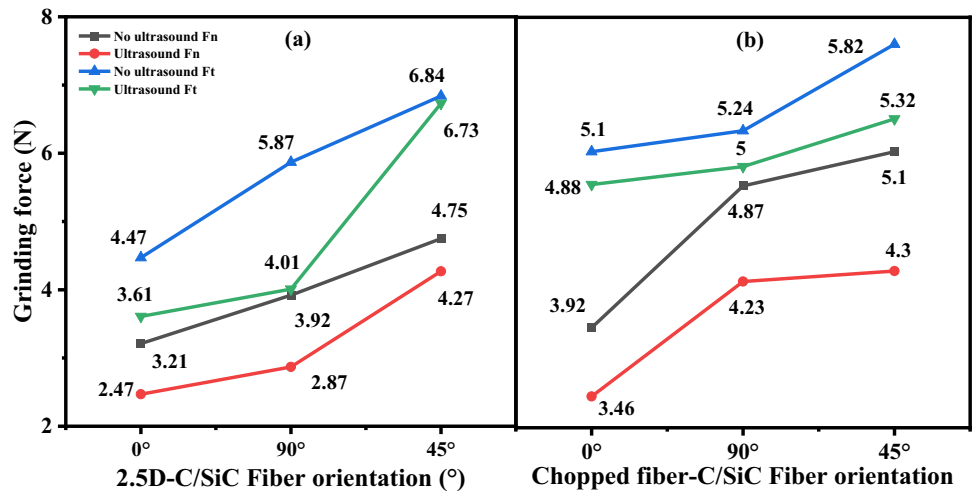
force of 0° fiber orientation is the least. This is due to the anisotropy and inhomogeneity of C/SiC composites, and the coefficient of friction of different fiber orientations is different. As a result, the fracture mechanical properties of different fiber orientations are different, so the grinding forces of different fiber orientations are also different. When C/SiC is ground in the direction parallel to the fiber, the fiber is axially compressed and then tears and breaks. As the toughness of the fiber is greater than that of the SiC matrix material, the grinding force required for brittle fracture is less. When C/SiC is ground in the direction perpendicular to the fiber, the fiber is fractured by the shear between the abrasive particles along the radial direction. Since the radial strength of the fiber is much greater than the axial strength, the breaking force of the fiber in radial shear is greater than the breaking force in axial extrusion. When the angle between the grinding direction and the C/SiC fiber is 45°, the abrasive particles must simultaneously overcome the axial compression fracture deformation and the radial shear deformation of the fiber. Therefore, the grinding force is satisfied: the grinding force of 45° fiber orientation is greater than that of 90° fiber orientation, and the grinding force of 0° fiber orientation is the least.

3.3.2 Effect of fiber orientation on surface quality

Figure 18 shows the effect of fiber orientation on surface roughness when grinding 2.5D-C/SiC and chopped fiber-C/SiC respectively. Figure 18 shows that the surface roughness of 2.5D-C/SiC is 45° fiber surface > vertical fiber surface > parallel fiber surface. Ultrasonic grinding can reduce the surface

roughness. The roughness of chopped fiber-C/SiC is as follows: parallel fiber surface > 45° fiber surface > vertical fiber surface. This is because the distribution structure of the two hardened fibers is different, the C/SiC material has anisotropy and inhomogeneity, and the friction coefficient of different fiber orientations is different, resulting in different fracture mechanical properties when grinding different fiber orientations. The surface roughness of different fiber orientations is also different. When 2.5D-C/SiC is ground parallel to the fiber direction, the fiber is torn and broken under the action of axial extrusion, and the broken fiber in this direction shows a relatively neat layering arrangement, so the surface roughness is minimal. When the cutting direction of the abrasive grain and the fiber angle is 45°, the abrasive grain has to overcome the axial compression and tearing deformation of the fiber and the radial shearing deformation at the same time, and both the transverse fiber layer and the longitudinal fiber fracture layer are arranged so that the surface roughness along the 45° fiber surface is the largest.

Figure 19 shows the surface microtopography magnified 1000 times. Figure 19a–c shows the morphology of the 2.5D-C/SiC parallel fiber plane, vertical fiber plane, and 45° fiber plane in sequence, which clearly shows the different fiber fracture mechanisms. In Fig. 19a, the fibers are first crushed and bow deformation occurs. Then bending deformation occurs along the axial direction of the fiber. As the axial load along the fiber continues to increase, the fiber tears until it breaks. In Fig. 19b, according to the stiffness principle, each flexible fiber is considered a rigid member with both ends constrained by fixed hinge supports. When uniform loads are applied in the direction perpendicular to the fiber, these uniform loads can be simplified as concentrated forces acting on the center of the fiber

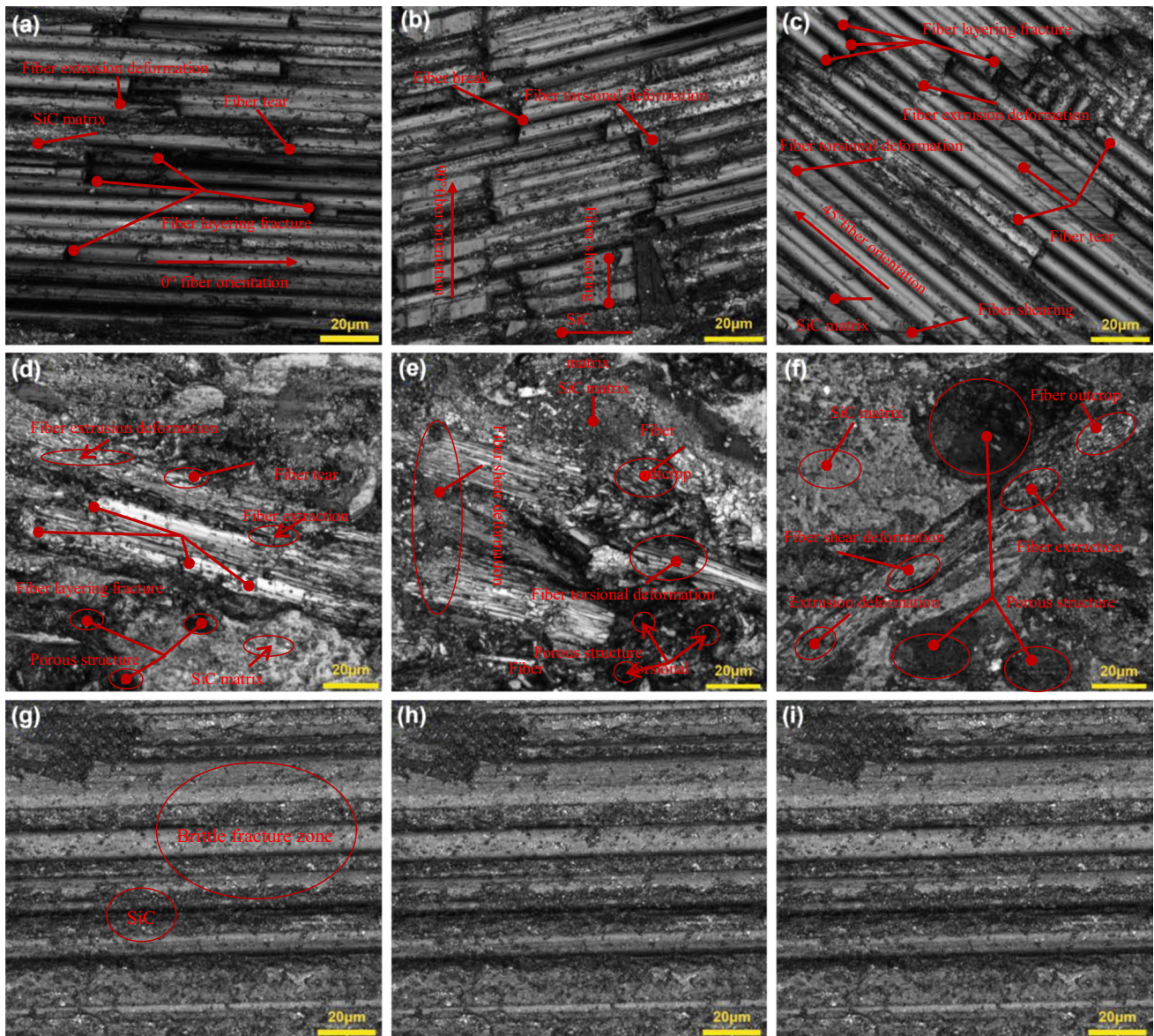**Fig. 18** C/SiC fiber orientation vs. surface roughness
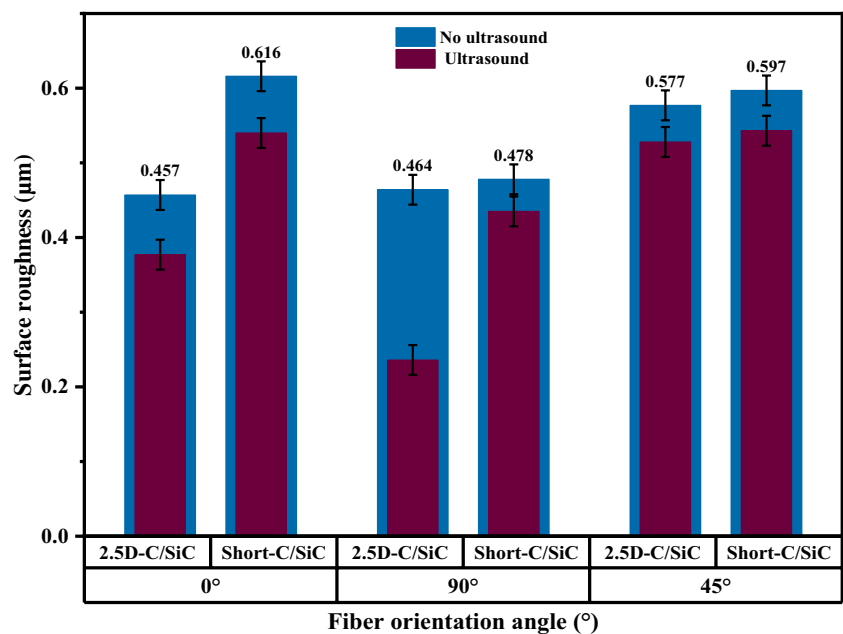
Fig. 19 Fiber orientation vs. surface morphology

rod. Under the action of the concentrated force, the elastic bending deformation along the radial direction of the single fiber occurs first. As the load is continuously increased, the fiber rod undergoes torsional and bending deformation due to the torque rotating around the fiber axis. The transverse fracture occurs along the radial direction of the fibers under shear action. The cross-section can be seen in Fig. 19b, and the fracture phenomenon is consistent with the theoretical analysis. In Fig. 19c, fibers are subjected to both compressive and shear stresses when ground along the 45° fiber direction. At the same time as the extrusion

deformation fibers peel and tear, torsional bending deformation will occur due to the effect of torque until the fibers break, forming chips and new surfaces. Figure 19d–f shows the surface topography of chopped fiber C/SiC. At the same magnification, a single chopped fiber is much thinner than a single 2.5D-C/SiC fiber. The surface of the tiny fiber has more rough edges and pores. Therefore, the surface roughness is poor. However, the fracture mechanism of the three directions is the same as that of 2.5D-C/SiC. Figure 19g–i shows the surface topography of SiC, and it is a surface formed by a brittle fracture.
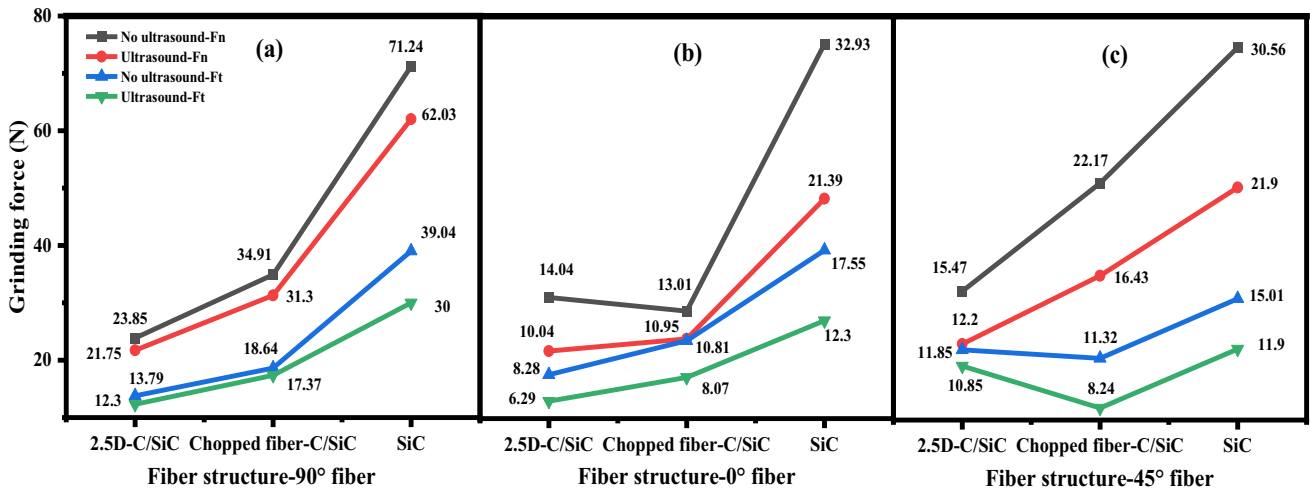
Fig. 20 Different fiber structure arrangements vs. grinding force

3.4 Effect of fiber structure arrangement on force and surface

3.4.1 Effect of fiber structure arrangement on force

Figure 20 shows the influence of different fiber structures on the grinding force. Under the same processing parameters, whether ultrasonic is applied or not, the grinding force is as follows: SiC > chopped fiber-C/SiC > 2.5D-C/SiC, and the grinding force of ultrasonic assisted grinding is smaller than that of non-ultrasonic grinding. One reason why the grinding force of SiC is greater than that of C/SiC is that the hardness of sintered SiC engineering ceramics is greater than that of C/SiC. C/SiC is produced by reactive melt infiltration of C/C composites, which may contain incomplete carbon in the

material. The reason why the grinding force of chopped fiber SiC is greater than that of 2.5D-C/SiC is that the carbon fiber in 2.5D-C/SiC is double-layered and the fiber is thicker than chopped fiber. The total amount of carbon fiber in 2.5D-C/SiC is relatively large, and the hardness of the carbon fiber is less than that of the SiC matrix, so the relative hardness of chopped fiber-C/SiC is greater than that of 2.5D-C/SiC.

3.4.2 Effect of fiber structure arrangement on the surface

Figure 21 shows the comparison of surface roughness between grinding 2.5D-C/SiC, chopped fiber-C/SiC, and SiC under the same parameters, which can be seen from the figure: the surface roughness is satisfactory: Chopped fiber-C/SiC > 2.5D-C/SiC > SiC and ultrasonic can reduce
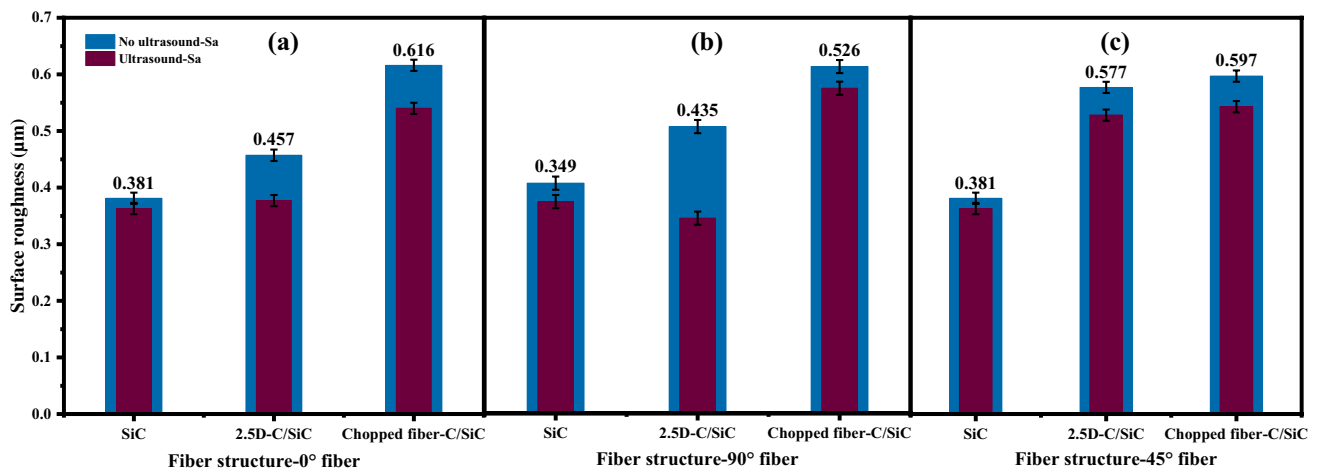

Fig. 21 Different fiber structure arrangements vs. surface roughness

the surface roughness. The reason why the roughness of C/SiC is greater than that of SiC ceramics is that the crisscross fibers laid in C/SiC materials increase the micro-convex and convex degree of the material surface. The fiber burrs on the surface after grinding C/SiC further increasing the surface roughness. The reason why the surface roughness of chopped fiber C/SiC is greater than that of 2.5D C/SiC is that the fiber layering in 2.5D C/SiC is regularly arranged and the fibers are continuous fibers with large diameters. The surface of chopped fiber C/SiC is composed of several small broken chopped fiber heads arranged in different rows. The two C/SiC surface morphologies show that the fiber heads on the 2.5D C/SiC surface are arranged in a more integrated manner. In contrast, the chopped fiber C/SiC structure has a larger porosity and more fine burrs, and the roughness after grinding is more obvious. Therefore, the surface roughness is as follows: chopped fiber-C/SiC > 2.5D-C/SiC > SiC.

4 Conclusion

The comparative test of grinding 2.5D C/SiC, chopped fiber C/SiC, and SiC were investigated. A series of results on the removal mechanism of C/SiC materials is obtained. Within the range of experimental parameters in this study, the experimental rules obtained are summarized as follows:

Based on two-dimensional ultrasonic auxiliary grinding kinematics analysis, applying two-dimensional ultrasonic auxiliary grinding C/SiC and SiC can cause abrasive particles to produce an elliptical motion trajectory. The use of auxiliary ultrasonic grinding can increase the contact arc length between the abrasive particles and the workpiece during grinding. Ultrasonic auxiliary grinding can decrease the maximum undeformed chip thickness in unit time.

This experiment had been drawn: two-dimensional ultrasonic auxiliary grinding 2.5D-C/SiC, chopped fiber-C/SiC, and SiC can reduce the grinding force, reduce surface roughness, optimize surface morphology, and improve the quality of the grinding surface and increase the ultrasonic amplitude when ultrasonic auxiliary grinding can reduce the grinding force. The maximum percentage reduction in normal and tangential grinding forces was 26.79% and 31.69%, respectively, when grinding 2.5D-C/SiC along 90° fiber orientation. The maximum percentage of ultrasound-assisted machining to reduce surface roughness was 37.93%, at which time the line speed for grinding 2.5D-C/SiC along 90° fiber orientation was taken as 10.48 m/s.

The single-factor experiment investigated the effects of various process parameters on the grinding force and surface quality during the grinding of three materials. It could be found that regardless of whether it was applied to an ultrasonic vibration assist grinding C/SiC. Within the range of this experiment, increasing the linear speed could reduce the grinding force, reduce the surface roughness, and improve the surface quality; reducing the grinding depth and feed speed could reduce the grinding force, reduce the surface roughness, optimize the surface morphology, and improve the surface quality.

The fiber orientation had a very important influence on the experimental results of C/SiC grinding. Whether it was grinding 2.5D-C/SiC or a chopped fiber-C/SiC, the grinding force is satisfied: orthogonal surface > longitudinal surface > transverse surface; for surface roughness, 2.5D-C/SiC satisfied orthogonal surface > longitudinal surface > transverse surface, chopped fiber-C/SiC satisfied: transverse surface > orthogonal surface > longitudinal surface.

2.5D-C/SiC, chopped fiber-C/SiC, and SiC belong to the brittle fracture mode during grinding. The fracture mechanism of C/SiC in different fiber structures was different. When the abrasive particles were parallel to the fiber direction, the fibers were subjected to tearing and crushing along the axial direction. The fiber was pulled out, the interfacial layer was damaged, the fiber tear was then broken, and the matrix crack was broken. When the abrasive particles were perpendicular to the fibers, the fiber was broken in the radicality of the shear effect between the abrasives. When the abrasive particles are at a 45° angle in the fiber direction, the fiber fracture occurs simultaneously in parallel and vertical fractures.

Compared with 2.5D-C/SiC, chopped fiber-C/SiC and SiC grinding phenomenon. Regardless of the ultrasound, it was applied, no matter what surface of the C/SiC. The grinding force satisfied the following: SiC > chopped fiber-C/SiC > 2.5D-C/SiC; surface roughness satisfied the following: chopped fiber-C/SiC > 2.5D-C/SiC > SiC.

References

1. Zhang LF, Wang S, Li Z, Qiao WL, Wang Y, Wang T (2019) Influence factors on grinding force in surface grinding of unidirectional C/SiC composites. Appl Compos Mater 26:1073–1085

2. Zhou YG, Tian CC, Jia SQ, Ma LJ, Yin GQ, Gong YD (2023) Study on grinding force of two-dimensional ultrasonic vibration grinding 2.5D-C/SiC composites material. Crystals 13(1):151

3. Li HB, Chen T, Duan ZY, Zhang YW, Li HT (2022) A grinding force in two-dimensional ultrasonic-assisted grinding of silicon carbide. J Mater Process Technol 304:117568

4. Ding K, Fu YC, Su HH, Chen Y, Yu XZ, Ding GZ (2014) Experimental studies on drilling tool load and machining quality of C/SiC composites in rotary ultrasonic machining. J Mater Process Technol 214:2900–2907

5. Xue F, Zheng K, Liao WH, Shu J, Miao DD (2021) Experimental investigation on fatigue property at room temperature of C/SiC composites machined by rotary ultrasonic milling. J Eur Ceram Soc 41:3341–3356

6. Zhang LF, Ren CZ, Ji CH, Wang ZQ, Chen G (2016) Effect of fiber orientations on surface grinding process of unidirectional C/SiC composites. Appl Surf Sci 366:424–431

7. Cao XY, Lin B, Zhang XF (2015) Investigations on the grinding process of woven ceramic matrix composite based on reinforced fiber orientations. Compos B 71:184–192

8. Du JG, Ming WY, Ma J, He WB, Cao Y, Li XK, Liu K (2018) New observations of the fiber orientations effect on machinability in grinding of C/SiC ceramic matrix composite. Ceram Int 44:13916–13928

9. Wang JJ, Zhang JF, Feng PF (2017) Effects of tool vibration on fiber fracture in ultrasonic machining of C/SiC ceramic matrix composites. Compos B 129:233–242

10. Zhai CT, Xu JK, Hou YG, Sun GB, Zhao BB, Yu HD (2022) Effect of fiber orientation on surface characteristics of C/SiC composites by laser-assisted machining. Ceram Int 48:6402–6413

11. Li YC, Ge X, Wang H, Hu YB, Ning FD, Cong WL, Ren CZ (2019) Study of material removal mechanisms in grinding of C/SiC composites via single-abrasive scratch tests. Ceram Int 45:4729–4738

12. Deng YH, Hou X, Li BC, Wang J, Zhang Y (2023) Review on mid-spatial frequency error suppression in optical components manufacturing. Int J Adv Manuf Technol 126(11–12):4827–4847

13. Ge J, Li W, Chao XJ, Wang HH, Wang ZW, Qi LH (2022) Experiment-based numerical evaluation of the surface recession of C/C–SiC composites under the high-energy laser. Ceram Int 48(23):34550–34563

14. Wang DP, Fan HJ, Xu D, Zhang YL (2022) Research on grinding force of ultrasonic vibration-assisted grinding of C/SiC composite materials. Appl Sci 12(20):1223–1239

15. Qin SQ, Zhu LD, Wiercigroch M, Ren TY, Hao YP, Ning JS, Zhao JZ (2022) Material removal and surface generation in longitudinal-torsional ultrasonic assisted milling. Int J Mech Sci 227:107375

16. Chen J, An QL, Chen M (2020) Transformation of fracture mechanism and damage behavior of ceramic-matrix composites during nano-scratching. Compos A 130:105756

17. Rosiger A, Goller R, Langhof N, Krenkel W (2021) Influence of in-plane and out-of-plane machines on the surface topography, the removal mechanism, and the flexural strength of 2D C/C-SiC composites. J Eur Ceram Soc 41:3108–3119

18. Zhu DH, Yan SJ, Li BZ (2014) Single-grit modeling and simulation of crack initiation and propagation in sic grinding using maximum undeformed chip thickness. Comput Mater Sci 92(1):13–21

19. Zhang MH, Pang ZX, Jia YX, Shan CW (2022) Understanding the machining characteristic of plain weave ceramic matrix composite in ultrasonic-assisted grinding. Ceram Int 48:5557–5573

20. Tian YB, Li LG, Fan S, Guo QJ, Cheng X (2021) A novel high-shear and low-pressure grinding method using specially developed abrasive tools. Proc Ins Mech EngPart B: J Eng Manuf 235:1–2

21. Liu B, Tian YB, Han JG, Li LG, Gu ZQ, Hu XT (2022) Development of a new high-shear and low-pressure grinding wheel and its grinding characteristics for Inconel718 alloy. Chin J Aeronaut 35(12):278–286

22. Tian YB, Li LG, Liu B, Han JG, Fan ZH (2020) Experimental investigation on the high-shear and low-pressure grinding process for Inconel718 superalloy[J]. Int J Adv Manuf Technol 107(7):3425–3435

23. Liu Q, Huang GQ, Xu XP, Fang CF, Cui CC (2018) Influence of grinding fiber angles on grinding of the 2D-Cf/C-SiC composites. Ceram Int 44(11):12774–12782

24. Xie ZW, Liu ZQ, Wang B, Xin MZ, Song QH, Jiang LP (2021) Longitudinal amplitude effect on material removal mechanism of ultrasonic vibration-assisted milling 2.5D-C/SiC composites. Ceram Int 47(22):32144–32152

25. Qu SS, Gong YD, Yang YY, Cai M, Sun Y (2018) Surface topography and roughness of silicon carbide ceramic matrix composites. Ceram Int 44(12):14742–14753

26. Qu SS, Gong YD, Yang YY, Wen XL, Yin GQ (2019) Grinding characteristics and removal mechanisms of unidirectional carbon fiber reinforced silicon carbide ceramic matrix composites. Ceram Int 45:3059–3071

27. Chen J, Ming WW, An QL, Chen M (2020) Mechanism and feasibility of ultrasonic-assisted milling to improve the machined surface quality of 2D Cf/SiC composites. Ceram Int 46(10):15122–15136

28. Luna GG, Axinte D, Novovic D (2020) Influence of grit geometry and fiber orientation on the abrasive material removal mechanisms of SiC/SiC Ceramic Matrix Composites (CMCs). Int J Mach Tools Manuf 157:103580

29. Jamshidi H, Nategh MJ (2013) Theoretical and experimental investigation of the frictional behavior of the tool–chip interface in ultrasonic-vibration assisted turning. Int J Mach Tools Manuf 65:1–7

30. Zhang MH, Pang ZX, Jia YX, Shan CW (2023) Understanding the machining characteristic of plain weave ceramic matrix composite in ultrasonic-assisted grinding. Ceram Int 48(4):5557–5573

31. Jamshidi H, Gurtan M, Budak E (2019) Identification of an active number of grits and its effects on mechanics and dynamics of abrasive processes. J Mater Proc Tech 273:116239

32. Xiao GJ, Zhuo XQ, Li SC, Chen BQ, Zhao ZY, Wang YX (2023) Study on surface creation law of planar two-dimensional ultrasonic-assisted abrasive belt grinding. J Mater Proc Tech 312:117847

33. Yan YY, Zhang YF, Zhao B, Liu JL (2021) Surface formation and damage mechanisms of nano-ZrO2 ceramics under axial ultrasonic-assisted grinding. J Mech Sci Technol 35(3):1187–1197

34. Yan YY, Liu LJ, Zhao B (2011) Study on the prediction of surface roughness of ZTA ceramics under ultrasonic assisted grinding. Adv Mater Res 1165(189–193):1325–1328

35. Yan YY, Zhao B, Liu JL (2010) Study on surface residual stress of nano-zirconia toughened alumina ceramics under two-dimensional ultrasonic vibration assisted grinding. Adv Mater Res 984(126–128):143–147

36. Tong JL, Zhao B, Yan YY (2009) Research on chip formation mechanisms of nano-composite ceramics in two-dimensional ultrasonic grinding. Key Eng Mater 416–416:614–618

37. Yan YY, Zhao B, Liu JL (2009) Research on the surface/subsurface damages of ZTA ceramics under two-dimensional ultrasonic vibration assisted grinding[J]. Key Eng Mater 416–416:619–623

38. Lawn BR, Swain MV (1975) Microfracture beneath point indentations in brittle. Solids J Mater Sci 10:113–122